Dalton Transactions

ROYAL SOCIETY OF CHEMISTRY

PAPER

View Article Online
View Journal

Cite this: DOI: 10.1039/d6dt00342g

Electron and spin density distributions and magnetic anisotropy in mixed-valent diruthenium(v) tetracarboxylates assessed *via* crystallographic and theoretical analyses

Sabrina Grenda, *[a] Haruki Yairi,[b] Torao Fujimoto,[b] Oscar Fabelo, [c] Iurii Kibalin, †[c] Nicolas Claiser, [e] Rémi Maurice, [f] Arsen Gukasov, [d] Laura Canadillas-Delgado, [c] José A. Rodriguez Velamazan, [c] Jean-François Jacquot,[g] Ryoji Mitsuhashi, ‡[h] Masahiro Mikuriya, [h] Makoto Handa *[b] and Dominique Luneau *[a]

The electron and spin density distributions of a tetracarboxylato mixed-valent diruthenium(II,III) complex, $(NBu_4)[Ru_2^{V}Br_2(O_2CC_3H_7)_4]$, were determined using high-resolution X-ray diffraction and polarized neutron diffraction (PND) on single crystals. Experimental and theoretical spin density distributions show that the spin density is predominantly localized on the ruthenium atoms, with partial delocalization onto bromide and carboxylate ligands. Charge-density analysis supports these findings, showing charge accumulation on the metal centres and typical donor–acceptor ligand–metal interactions. The experimental topological analysis of the Ru···Ru bond confirms an open-shell metal–metal interaction. Local magnetic anisotropy was explored through angle-resolved magnetic susceptibility measurements and PND. Magnetic data reveal significant magnetic anisotropy, with an easy axis along the crystallographic *c* axis and a hard magnetization axis along the crystallographic *b* axis. Local magnetic susceptibility tensors derived from PND highlight pronounced planar magnetic anisotropy oriented along the equatorial Ru–O plane. The experimentally determined anisotropy parameters are in excellent agreement with *ab initio* calculations.

Received 9th February 2026,
Accepted 2nd April 2026

DOI: 10.1039/d6dt00342g

rsc.li/dalton

Introduction

The first mixed-valence tetracarboxylato diruthenium(II,III) compound $[Ru_2^{V}(O_2CC_3H_7)_4Cl]_n$ with a lantern-type structure of the tetra-*n*-butyratodiruthenium core, or paddlewheel structure as called today, was discovered six decades ago.[1] The analysis of structural features using X-ray diffraction on a single crystal showed that the two ruthenium ions are equivalent with a short Ru–Ru distance (2.28 Å), suggesting an average oxidation state of +2.5 for each ruthenium ion and the presence of an Ru–Ru bond.[2] At this time, this brought a support to the freshly identified quadruple and δ bonds by Cotton.[3,4] Subsequently, numerous investigations were carried out to elucidate the electronic configuration of such systems. These comprised electronic, Raman and EPR spectroscopies and magnetic studies[5–9] as well as the synthesis of many other diruthenium tetracarboxylate compounds bearing different carboxylates and different anions in their axial positions.[10–12] All studies agreed with a delocalized mixed-valence-type system belonging to class III of the Robin-Day classification.[13] The electronic configuration was established as $\sigma^2\pi^4\delta^2(\delta^*\pi^*)^3$ in the molecular orbital approach.[7,14] This means that, among the 11 electrons provided by the d^5 and d^6 configurations of the Ru(III) and Ru(II), there are 8 electrons that fill the quadruple bond ($\sigma^2\pi^4\delta^2$) while the three remaining unpaired electrons are distributed by an accidental degenracy in the π* and δ*

[a]*Laboratoire des Multimatériaux et Interfaces (UMR CNRS 5615), Université Claude Bernard Lyon 1, 69100 Villeurbanne 69100, France.*
E-mail: dominique.luneau@univ-lyon1.fr
[b]*Department of Chemistry, Graduate School of Natural Science and Technology, Shimane University, 1060 Nishikawatsu, Matsue 690-8504, Japan*
[c]*Institut Laue-Langevin, 71 avenue des Martyrs, 38042 Grenoble Cedex 9, France*
[d]*Laboratoire Léon Brillouin (LLB), CEA-CNRS (UMR CNRS 12), CEA. Saclay, 91191 Gif-sur-Yvette, France*
[e]*CRM2 (UMR CNRS 7036), Université de Lorraine, BP70239, 54506 Vandoeuvre-les-Nancy, France*
[f]*Univ Rennes, CNRS, ISCR (Institut des Sciences Chimiques de Rennes) – UMR 6226, 35000 Rennes, France*
[g]*CEA-Grenoble, 38054 Grenoble, France*
[h]*School of Science and Technology, Kwansei Gakuin University, Sanda, 669-1330, Japan*
† Present address: European Spallation Source ERIC, P.O. Box 176, SE-221 00 Lund, Sweden.
‡ Present address: Institute of Liberal Arts and Science, Kanazawa University, Kakuma, Kanazawa 920-1192, Japan.

orbitals. This gives a formal bond order of 5/2 in the ground configuration. The result is thus an unusual high-spin $S = 3/2$ state for the whole diruthenium core. This is why it is better formulated as diruthenium(v) than diruthenium(ii,iii). In addition, the three unpaired electrons in the accidentally degenerated π^* and δ^* orbitals[2] cause a large zero-field splitting (ZFS) with strong axial parameter $D = 60–80$ cm^{-1}.[2,7,9,10–12,12,15–17]

The peculiar electronic structure of diruthenium tetracarboxylate compounds, combining a high-spin state of $S = 3/2$ with large magnetic anisotropy together with the possibility of exchanging ligands in the axial positions, has prompted their use as building blocks for molecule-based magnets. One-, two- and three-dimensional systems have been reported, which are constructed from diruthenium tetracarboxylates alone or bridged by paramagnetic linkers in axial positions, such as nitroxide radicals or hexacyanidometalate ions $[M(CN)_6]^{3-}$.[10,15,18–21] Among these systems, the one-dimensional chains present in the pivalate derivative $(PPh_4)_2[Ru_2(O_2C(CH_3)_3)_4W(CN)_8]$, previously reported by our group, exhibit a high ordering temperature ($T_c = 44$ K)[20] and represent one of the best examples of high-spin diruthenium(v) tetracarboxylate compounds. Improving the performance of these molecule-based magnets requires a detailed knowledge of their magneto-structural relationships at the molecular level, and this raises two main questions that we address in this study.

A first question is how large the spatial distribution of the unpaired electron density is between the ruthenium atoms and onto the carboxylate and axial ligands. Early theoretical calculations have tentatively answered this question,[7] and we have previously reported a ^{13}C NMR study that agreed with partial spin delocalization onto the carboxylate groups.[22] In this work we revisit this question by experimentally mapping the electron and spin density distributions in a diruthenium(v) tetracarboxylate compound, $(NBu_4)[Ru_2^V(O_2CCH_3)_4Br_2]$. This was achieved using high-resolution X-ray diffraction (XRD) and polarized neutron diffraction (PND) on single crystals. High-resolution XRD is a powerful crystallographic technique that enables precise experimental model of electron density distributions within a crystal using multipole refinement.[23–25] The resulting deformation density, that is, the deviation from the spherical atom model, allows for visualization of the bonding and charge localization.[26] This can be complemented by calculating the Laplacian ($\nabla^2\rho$) of the electron density to highlight the regions of charge concentration and depletion and provide insights into the bond character.[27] Furthermore, topological analysis based on the quantum theory of atoms in molecules (QTAIM)[28] identifies especially critical points corresponding to bonding interactions and gives access to atomic charges.[29] A full multipolar model can also provide access to a precise calculation of the electrostatic potential, offering insights into interatomic electrostatic interactions, including energetic aspects.[30] Thanks to the neutron magnetic moment, PND on single crystal is a best suited crystallographic technique to probe magnetic compounds at the atomic level.[31] PND has proven to be particularly powerful to map spin density in molecular and coordination compounds, where it may spread outside the magnetic centres, such as in ligands.[32] Beyond this, PND provides direct information on the relationship between crystal structure and magnetic interaction pathways.[33–37]

A second important question, with diruthenium tetracarboxylate compounds, is how large is the molecular magnetic anisotropy and how its principal magnetic axis are oriented a with respect to the molecular geometry. Indeed knowledge of such magneto-structural relationships is important because magnetic anistropy determines the size of the remanant magnetization and the coercive field of the molecule-based magnets.[38,39] Magnetic anisotropy can be measured by different experimental techniques such as electron paramagnetic resonance (EPR). However, the determination of the orientation of the principal magnetic axis is challenging. To address this question, we also used PND data on single crystals within the local susceptibility tensor approach.[40] We have previously shown that this method allows the fine determination of the direction and strength of the local principal magnetic anisotropy axes on metal ions.[41–46] Our results reveal an unprecedented view of the charge and spin distribution as well as of the magnetic anisotropy in diruthenium tetracarboxylate systems which is supported by quantum mechanical calculations.

Results and discussion

We initiated the study with the tetra-pivalate diruthenium dithiocyanato compound, $[NBu_4][Ru_2^V(O_2C(CH_3)_3)_4NCS_2]$,[20] then the tetra-acetate dichloro derivative, $[NBu_4][Ru_2^V(O_2CCH_3)_4Cl_2]$.[22] Both compounds could be grown as large single crystals suitable for PND. However, they incorporated crystallization solvents that escaped during the experiments, preventing reliable data collection. Driven by our continued interest in diruthenium tetracarboxylate systems, we then turned to the *n*-butyrate derivative with bromido ligands in the axial positions, which finally yielded large, solvent-free, stable single crystals of $(NBu_4)[Ru_2^V(O_2C_3CH_7)_4Br_2]$, enabling successful neutron diffraction measurements. Moreover, this compound is one of the few diruthenium tetracarboxylates featuring bromido ligands.[47–51]

High-resolution X-ray diffraction crystal structure

Tetra-*n*-butylammonium tetra-*n*-butyratodibromidodiruthenium $(NBu_4)[Ru_2^V(O_2CC_3H_7)_4Br_2]$ crystallises in the triclinic $P\bar{1}$ space group. Crystal data and structure refinement parameters, obtained from high-resolution XRD on a single crystal at 100 K, are summarised in Table S1. The asymmetric unit comprises two halves of centrosymmetric diruthenium anion complexes $[Ru_2^V(O_2CC_3H_7)_4Br_2]^-$ labelled A and B plus one tetra-*n*-butylammonium counter-cation (NBu_4) for electroneutrality. A terminal carbon atom (C4) of one butyl chain of the tetrabutylammonium cation (NBu_4) was refined as disordered on two positions. Each tetra-*n*-butyratodirutheniumdibromido anion, $[Ru_2^V(O_2CC_3H_7)_4Br_2]^-$, A and B, possesses a crystallographic inversion centre at the midpoint of the diruthenium core, with two equivalent ruthenium ions coordinated in the equatorial plane by four bridging tetra-*n*-butyrato ligands in the so-called

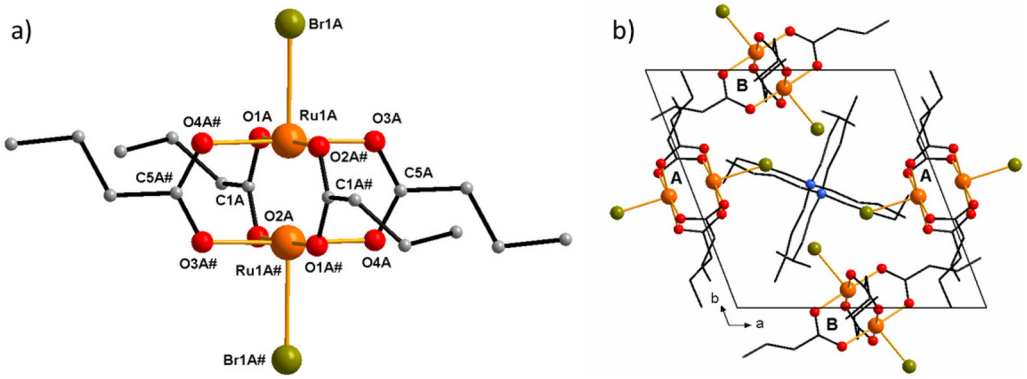

Fig. 1 (a) Representation of the $[Ru_2^{V}(O_2CC_3H_7)_4Br_2]^-$ anion complex unit labelled A. (b) View along the *c* axis of diruthenium A and B in the unit cell. Hydrogen atoms are omitted for clarity.

paddlewheel fashion. As shown in Fig. 1 and Fig. S1 for units A and B, bromido ligands complete the coordination of both ruthenium ions in axial positions. The major difference between the dinuclear units A and B lies in the conformation of the *n*-butyl chains of the *n*-butyrato ligands: both *cis* and *trans* conformations are shown by A, whereas only the *trans* conformation is displayed by B (Fig. S2). The structural features are very close to those reported by Cotton for the first tetracarboxylato diruthenium complex as well as for other tetracarboxylato diruthenium complexes.[2] The four oxygen atoms, located in the equatorial plane of each ruthenium, are strictly coplanar, and the ruthenium ions are slightly out of the plane (Ru1A: 0.035 Å, Ru1B: 0.033 Å). Consistent with earlier studies, the Ru–Ru distances exceed the mean O–O distance in the carboxylate group (Table S2) and are in the range observed for diruthenium(II,III) tetaracarboxylato complexes (2.27–2.31 Å).[10–12,47–51] The Ru–Br bond lengths (Table S2) are similar to those in other tetracarboxylatodibromidodiruthenium complexes.[47–51] Comparatively, they are longer than the Ru–Br bond lengths usually observed in bromido complexes of Ru^{3+} and Ru^{2+} complexes. This makes the substitution of the axial ligands easy, as already pointed out by Cotton.[2] Moreover, the Ru–Br bonds in the dibromido isolated complexes are comparatively shorter than those in bromido-bridged chain complexes, making the Ru–Ru distances in dibromido isolated complexes (2.2998(19)–2.3124(11) Å) a little longer than those found in bromido-bridged chain compounds (2.2850(6)–2.2906(7) Å).[47–51]

Electron density model

The static deformation density maps calculated as the difference between the multipolar and independent atom models show positive deformation densities along the C–O and C–C bonds of the carboxylate ligand as expected (Fig. 2a and Fig. S3a–d).[52] For both diruthenium complexes A and B, the lone pairs of the oxygen atoms are pointing toward the ruthenium centre. As shown in Fig. 2a and Fig. S3, an accumulation of electron density on the ligands is observed, together with depletion at the metal centres, consistent with previous

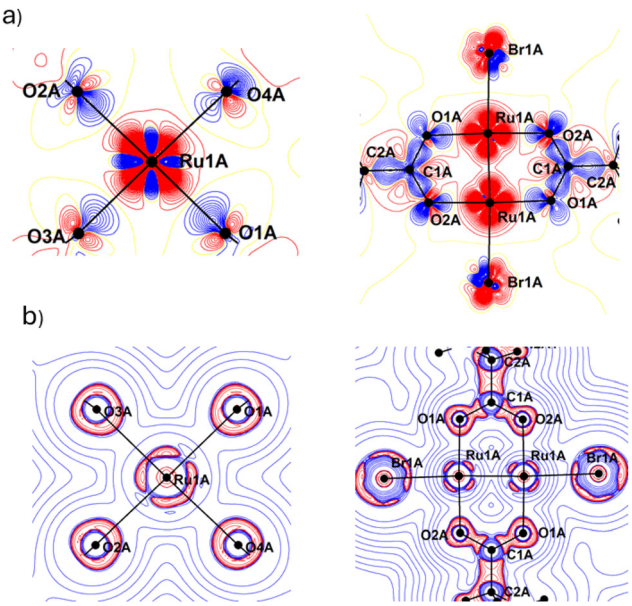

Fig. 2 (a) Static deformation density map of the dimer A (blue = positive, red = negative, and yellow = zero contour). Isocontour lines are separated by 0.05 e A^{-1}.[3] (b) Laplacian of the electron density of diruthenium A (blue = positive, red = negative; contour at $\pm 2^n$ e $Å^{-5}$).

reports for other metal complexes and in agreement with the concept of a donor–acceptor ligand–metal bond.[26,53,54] The electron density over each ruthenium centre is similar in both A and B diruthenium complexes and has a cross shape comprising six negative lobes and four positive lobes (Fig. S4). Five of the negative lobes point toward the ligands, while the sixth is pointing directly toward the Ru···Ru bond. The four positive lobes (Fig. S3e and f) are oriented along diagonal directions (Fig. S4). Along the Ru···Ru bond, there is no pronounced charge accumulation.[55]

The Laplacian maps (Fig. 2b and Fig. S5) clearly evidence valence shell charge concentrations (VSCCs) and valence shell charge depletions (VSCDs). The C–O bond shows the expected features of a normal covalent bond,[52] and the valence shell

charge concentration (VSCC) at the carbon and oxygen atoms indicates an sp^2 valence configuration. The donor character of the oxygen lone pair toward the Ru atom is confirmed by the charge concentrations on the oxygen atoms, as expected for a metal–ligand coordination bond.[52] For both A and B diruthenium complexes, there are four VSCCs and six VSCDs around each Ru atom, as shown in Fig. 2b and Fig. S5a–d, with the VSCCs located in between the Ru–O bond directions.[55] The valence shell of the ruthenium atoms reflects an uneven population among the five d orbitals and indicates preferential occupation of the t_{2g} and e_g orbitals.[54,56]

The topological analysis of the electron density[29] for Ru–O and Ru–Br interactions is in agreement with polar covalent bonds (Table S5). Considering the middle of the bonds, the positions of the bond critical points (BCPs) of the Ru–O bonds have an average shift of 0.7 Å away from the Ru atoms and toward the O atoms, indicating slight polarization.[53] The metal–ligand bonds have similar topological properties at the BCPs, with an average density of ρ = 0.32 e Å^{-3} for Ru–Br and ρ = 0.70 e Å^{-3} for Ru–O, with positive Laplacian values ($\nabla^2\rho$ = 3.9 e Å^{-5} for Ru–Br and $\nabla^2\rho$ = 11 e Å^{-5} for Ru–O). The value of the ellipticity ε, with an average of 0.01 for Ru–Br and 0.12 for Ru–O, is in agreement with a single covalent bonding. The topological properties of the Ru–L bonds are comparable to those of other related metal–ligand interactions.[53,54,57] For the Ru···Ru interactions, the BCP is localized at the midpoint between the two ruthenium atoms. The small value of the electron density at BCP (ρ = 0.50 e Å^{-3}), the positive value of the Laplacian ($\nabla^2\rho$ = 8.3 e Å^{-5}), the positive value of G_{cp}/ρ (0.19 he^{-1}) but smaller than unity and the small negative value of G_{cp}/ρ (−0.02 he^{-1}) are consistent with an open-shell metal–metal interaction.[58,59] The high value of the Laplacian ($\nabla^2\rho$ > 1 e Å^{-5}) appears inadequate for the classification of the M–M bond, but increase of the Laplacian at the BCP has already been reported for metal–metal bond orders greater than unity.[60,61] An experimental value of $\nabla^2\rho$ = 31.62 e Å^{-5} has also been reported in the study of the quintuply bonded dichromium complex $Cr_2(dipp)_2$.[52]

The complementary analyses of the experimental electron density in $(NBu_4)[Ru_2^{V}(O_2CC_3H_7)_4Br_2]$, derived from high-resolution XRD, provide a detailed mapping of the electron distribution that agrees well with previous studies on tetracarboxylato diruthenium(v) complexes and with a delocalized class III mixed-valence system in the Robin-Day classification.[13] The electron distribution in both diruthenium moieties A and B was found to be largely similar, as were the atomic charges (Table S4). The main difference was found in the refinement of the parameter κ' (Table S3), which converged to a slightly higher value for Ru1B (1.41) than for Ru1A (1.20). Since the κ and κ' parameters control the radial expansion/contraction of the outer shell within the multipole model, this higher value for Ru1B reflects a more contracted outer shell compared to Ru1A.[23–25] It is noteworthy that this is consistent with a similar difference between Ru1A and Ru1B that we observed in the refinement of magnetic anisotropy from the PND data, as reported below.

Magnetic studies

Magnetic measurement on a polycrystalline sample yield a value of the product of magnetic susceptibility and temperature (χT) of 2.16 cm^3 K mol^{-1} at 300 K (Fig. 3a). This is close to the spin-only value expected for three unpaired electrons (χT = 1.875 cm^3 K mol^{-1}) in accordance with the electron configuration of $\sigma^2\pi^2\delta^2(\pi^*\delta^*)^3$. Upon cooling, the χT product decreases continuously to 1.40 cm^3 K mol^{-1} at 2 K (Fig. 3a).

The magnetic data were well simulated with parameters, g = 2.16 and D = 83 cm^{-1} using the previously reported analytical expressions for diruthenium tetracarboxylate.[18] These values are similar to those reported for other lantern-type diruthenium(v) complexes.[9,12,15–17] The implementation of intermolecular interactions between the diruthenium complexes within the molecular field approximation (zJ),[12,62] did not improve the quality of the fit and was considered negligible as the closest intermolecular Ru···Ru distance in the crystal is 8.2935(11) Å. The field dependences of the magnetization at different temperatures is also well simulated (Fig. 3b) with these parameters.

Further angle-resolved susceptibility measurements were performed on a single crystal of 3.5 × 2.5 × 1.5 mm^3 at 2 K under a magnetic field of 0.1 T, as shown in Fig. S6. Rotation of the crystal around the a and b crystallographic axes perpendicular to the magnetic field clearly shows the existence of a significant magnetic anisotropy, with the easy magnetization axis preferentially along the c axis. The hard magnetization axis is mainly along the b axis. However, due to the presence of two dimers A and B in the unit cell, the molecular principal magnetic axes of each dimer cannot be deduced from these angle-resolved measurements.

Spin density model

The study of the spin density was carried out by polarised neutron diffraction (PND), as it is the best method to gain insight into the possible delocalisation of unpaired electrons towards the ligands and between the ruthenium atoms. Flipping ratios were collected on the D3 diffractometer at the Institute Laue–Langevin (ILL) at 2 K under an applied magnetic field of 9 T.[31] The nuclear structure factors were obtained from neutron diffraction measurements performed at the same temperature on the D19 diffractometer at the ILL.

The PND data were analysed using the model-free maximum entropy method (MEM), which is known to provide much more reliable results than conventional Fourier syntheses by significantly reducing both noise and truncation effect.[63,64] However, it should be noted that, in magnetically anisotropic compounds, MEM reconstructs only the component of the magnetization density along the applied magnetic field, which allows only for a qualitative localization of unpaired electrons within the unit cell. As the local symmetry of the magnetic ions is the same as the overall symmetry of the crystal, the same symmetry paramagnetic space group $P\bar{1}$ was used for the reconstruction of spin density. The results of the reconstruction are presented in Fig. 4 and Fig. S7.

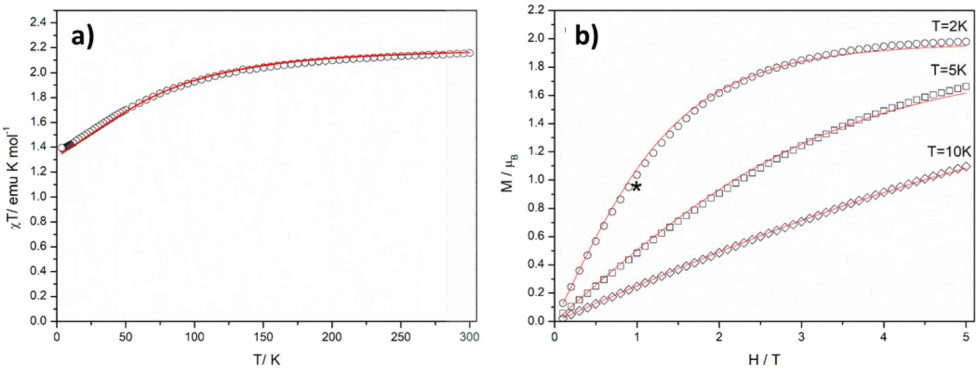

Fig. 3 (a) Experimental (○) temperature dependence of $\chi_M T$ for **1** and (b) field dependence of the magnetization at 2 K (○), 5 K (□) and 10 K (◊). The red solid lines denote the simulated curve using the parameters of g = 2.13, D = 83 cm^{-1}, and zJ = 0 cm^{-1}. The magnetization estimated from local susceptibility tensors measured by PND data is shown by a star symbol.

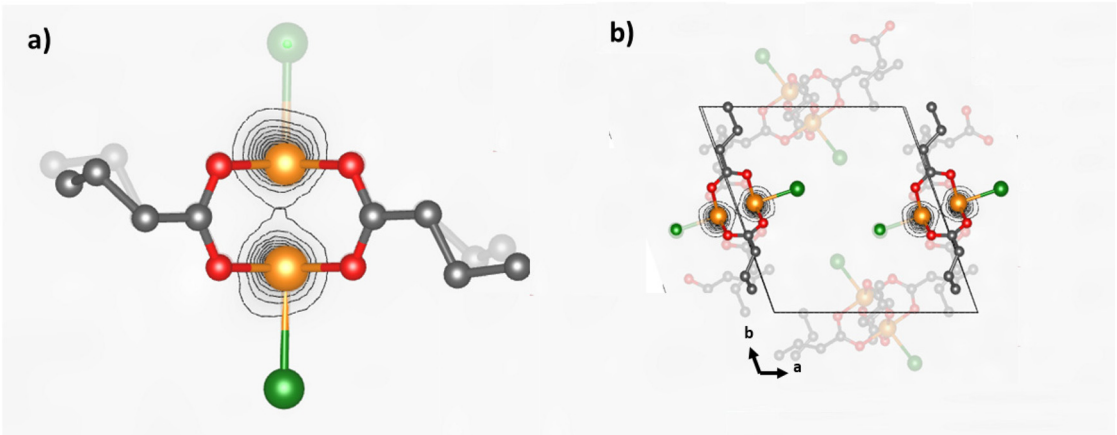

Fig. 4 Experimental spin density at 2 K under a magnetic field of 9 T applied nearly along the c-axis for diruthenium A: (a) projection around the Ru–Ru bond. (b) Projection of the unit cell along the [001] direction. Contour levels are fixed at 0.035μ_B A^{-3}.

From the distribution measured in the saturated regime, it appears that the spin density is mainly located on the Ru atoms of the diruthenium complexes (Fig. 4 and Fig. S7), with almost no significant spin densities on the ligands.

Magnetic susceptibility tensor

PND was also used to determine the local magnetic anisotropy by the local susceptibility tensor method.[40,44] In these experiments, flipping ratios were collected on the D3 diffractometer at the ILL at 2 K under a magnetic field of 1 T, and for three different orientations of the crystal, from which the magnetic susceptibility tensors of each Ru ion of the two diruthenium complexes A and B were determined:

$$\chi_{RuA} = \begin{pmatrix} 0.25(3) & 0.03(3) & 0.02(2) \\ 0.03(3) & 0.64(7) & -0.01(2) \\ 0.02(2) & -0.01(2) & 0.65(1) \end{pmatrix} \frac{\mu_B}{T}$$

$$\chi_{RuB} = \begin{pmatrix} 0.61(3) & 0.09(3) & -0.04(2) \\ 0.09(3) & 0.07(7) & 0.10(2) \\ -0.04(2) & 0.10(2) & 0.66(1) \end{pmatrix} \frac{\mu_B}{T}$$

The tensors are defined in the right-hand Cartesian coordinate system XYZ: Z is aligned along the crystallographic c axis and X is aligned along the reciprocal crystallographic a^* axis. The experimental error bars are given in brackets. They are represented in the form of magnetization ellipsoids in Fig. 5. This clearly shows a planar-type anisotropy oriented towards the oxygen planes for both dimers and indicates a significant influence of oxygen on the magnetic anisotropy of the Ru ions.

Diagonalization of the magnetic susceptibility tensors yields the following eigenvalues for the main axes of magnetic anisotropy of Ru1A and Ru1B:

$$\chi_{A1} = 0.24\mu_B\ T^{-1}, \quad \chi_{A2} = 0.64\mu_B\ T^{-1}, \quad \chi_{A3} = 0.65\mu_B\ T^{-1}$$

$$\chi_{B1} = 0.04\mu_B\ T^{-1}, \quad \chi_{B2} = 0.62\mu_B\ T^{-1}, \quad \chi_{B3} = 0.69\mu_B\ T^{-1}$$

This confirms a planar magnetic anisotropy, which is almost "flat" for Ru1B, with the easy-plane susceptibility, corresponding to the oxygen plane, being around 0.65μ_B T^{-1} for Ru1A and Ru1B. A small transverse susceptibility is observed for Ru1A (χ_{A1} = 0.24μ_B T^{-1}), but it is almost zero for Ru1B (χ_{B1} = 0.04μ_B T^{-1}).

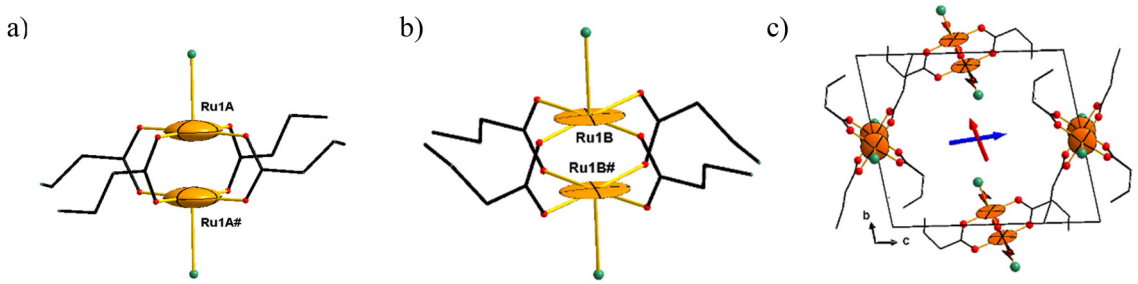

Fig. 5 Magnetization ellipsoids at the Ru sites measured at 2 K under 1 T in the unit cell. The orientation of the magnetization ellipsoid according to the molecular frame is shown for the dimer A (a) and dimer B (b). The easy and hard magnetization axes of the sample are indicated by blue and red arrows, respectively (c).

Based on the refined susceptibility tensors, the estimated easy magnetization axis of the crystal is oriented mainly along the crystallographic *c* axis: $-0.01X + 0.15Y + 0.99Z$ (blue arrow in Fig. 5c), while the hard magnetization axis is mainly oriented along the *b*–*a* direction: $-0.46X + 0.88Y - 0.14Z$ (red arrow in Fig. 5c).

From the summation of the χ_{RuA} and χ_{RuB} tensors, the angular-resolved susceptibility and magnetization of the sample were calculated (see details in the SI). The e stimated sample magnetization at an applied field (1 T) along the main crystallographic axis agrees well with magnetic measurements within error bars (Fig. S6b). Simulation of the angular-resolved susceptibility demonstrates quite good agreement with experimental data measured at 0.1 T (Fig. S6a).[42] The orientations of the easy and hard magnetization axes are correctly predicted. The small disagreement in the absolute values between predictions and experiment is attributed to the fact that the magnetization curve is outside the linear region at a field of 1 T, at which the PND measurements were performed. The calculated powder-averaged magnetization ($0.48(7)\mu_B$ per ion) is in excellent agreement with the magnetization measured on the powder sample at 2 K (Fig. 3b). Thus, the local susceptibility tensors measured by PND well describe the magnetometry data.

It is important to emphasize that such a precise determination of the magnetic anisotropy is not possible by magnetometry. Only PND can provide the local susceptibility tensors and the anisotropies on each magnetic ruthenium centre. Thus, if one hypothesis the mixed-valence diruthenium as being localised, class I or class II of the Robin-Day classification, then the Ru^{2+} and Ru^{3+}metal centers, could be distinguishable by PND because their magnetic moments are significantly different. Moreover, in such a case this would break the inversion symmetry center of the dimer. Nevertheless, decreasing the space group to *P*1 does not improve the quality of refinement. This is another confirmation that, in each diruthenium, the two ruthenium atoms are equivalent, in full agreement with previous reports and with analyses of charge-density distribution.[1–12,14]

However, although the two ruthenium atoms in each diruthenium are equivalent, there are differences between the two diruthenium units in their (de)localised character. As we just discussed, although the anisotropies of Ru1A and Ru1B are both planar, that of Ru1B is much flatter (Fig. 5). Indeed, as with the determination of electron density, refinement of the magnetic anisotropy at the ruthenium sites results in κRu1A = 1.03(1) and κRu1B = 1.17(2), which indicates that it is slightly more contracted for diruthenium B than for diruthenium A. Given that these studies were conducted independently on different crystals, a small crystal for charge-density measurements and a large one for magnetic anisotropy, we believe that this difference between Ru1A and Ru1B is meaningful. Thus, the contraction effect we observed in both experiments for Ru1B suggests that diruthenium B may be slightly more localized than diruthenium A. In other words diruthenium B is a delocalised mixed-valence of class III, with spin $S = 3/2$ in agreement with magnetism, but somewhat closer to a localised case, as has been previously argued for some other borderline mixed-valence complexes.[65]

Quantum mechanical calculations

The fine description of the nature of many-electron states in transition-metal complexes may require the use of multiconfigurational quantum-mechanical calculations. To obtain a qualitatively correct view on the bonding pattern in the complex of interest and to derive an accurate description of the (molecular) anisotropy of the complex, we therefore employed only multiconfigurational and multireference wavefunction approaches (see the SI for computational details).

We start our analysis with a bonding analysis in terms of the effective bond order.[66] As mentioned in the Introduction, the ground-state electronic configuration in the valence space of the two ruthenium centres is $\sigma^2\pi^4\delta^2(\delta^*\pi^*)^3$, which corresponds to a formal bond order of 5/2 (eight bonding and three antibonding electrons). A state-specific calculation with complete active space self-consistent field (CASSCF) allows to define an effective bond order. The active space comprizes 11 electrons within 10 orbitals (corresponding to the bonding and antibonding combinations of the metal d orbitals). The electronic configuration of the ground state at the CASSCF level is $\sigma^{1.88}\pi^{3.76}\delta^{1.85}\delta^{*1.14}\pi^{*2.22}\sigma^{*0.12}\delta^{0.01}\delta^{*0.01}$, from which an effective bond order of 2.01 is obtained. The σ (0.88) and π (0.77) contributions to this bond order are in perfect line with

previous findings for diruthenium(II) compounds,[67] while the extra electron withdrawal here favours the emergence of a δ partial bond (0.36), resulting in a higher (effective) bond order. These results arise from calculations performed on diruthenium A. Results for diruthenium B are reported in the SI. As expected, no significant changes are observed in the computed properties of diruthenium B because the two complexes (A and B) show minor structural differences (calculations were based on the experimental crystallographic structures) (Table 1).

The Mulliken atomic spin densities were then determined for this spin–orbit-free ground state at the CASSCF level and from spin-unrestricted DFT calculations using B3LYP.[68–70] As expected, the spin density is more delocalized at the spin-unrestricted B3LYP level than at the CASSCF level. Nevertheless, both evidence a larger spin delocalization onto each Br atom than onto each O atom, meaning that these results are robust with respect to the applied quantum mechanical method.

It turns out that the spin density is essentially localized on the Ru atoms (1.438 each) and then moderately propagated onto the ligands (0.014 per Br atom, 0.011 per O atom, and 0.003 on each C atom bridging two coordinated O atoms). No distinction is observed between the two Ru atoms based on the atomic spin densities; the system effectively behaves as a typical class III mixed-valence compound. Unlike the atomic charges which are strongly dependent on the underlying charge model and also of the employed level of theory, the atomic spin populations are quite robust. Therefore, we are quite confident in the observed trend (more delocalization on the Br *vs.* O atoms).

In view of further computing the zero-field splitting of the ground $S = 3/2$ state by means of the established spin–orbit configuration interaction technique combined with the effective Hamiltonian theory,[71] we computed several spin–orbit-free excited states. A good compromise between accuracy, computational cost, and minimization of state-averaging artefact was obtained for a set of 13 $S = 3/2$ and 16 $S = 1/2$ spin–orbit-free states (see the SI for more details). At the N-electron valence state second-order perturbation theory (NEVPT2) level,[72,73] the ground $S = 3/2$ state lies 0.91 eV below the first excited $S = 3/2$ state and 0.29 eV below the first (excited) $S = 1/2$ one. Once the spin–orbit coupling is introduced, the lowest two Kramers doublets are split by 188 cm^{-1} (23.2 meV), and the extracted zero-field splitting parameters are $D = 94$ cm^{-1} and $E = 2$ cm^{-1}, in good agreement with experiment. The hard axis of magnetization almost perfectly coincides with the Ru–Ru orientation, which is unsurprising given the paddlewheel structure. By employing the effective Hamiltonian theory, we project the *ab initio* wave functions on the model space. Here, the model space consist of the four spin components of the ground spin-quartet state. The projection of the *ab initio* wave functions on these components is 96.6% for the ground Kramers doublet and 99.1% for the excited Kramers doublet. Therefore, the spin-orbit coupling is not expected here to significantly reduce the effective bond order[74] meaning that the previous value, 2.01, obtained at the scalar-relativistic level and indicative of an effective double bond, is confirmed.

Table 1 Atomic spin densities obtained at the CASSCF level from spin-unrestricted DFT calculations with the B3LYP exchange–correlation functional

Complex		Ru	Br	O	C (carboxylate)
A	CASSCF	1.438	0.014	0.010; 0.011	0.003
	B3LYP[68–70]	1.379	0.065	0.028; 0.030	−0.029
B	CASSCF	1.438	0.013	0.010; 0.011	0.003
	B3LYP[68–70]	1.381	0.062	0.028; 0.030	−0.029; −0.030

Conclusion

The combined analysis of spin density by PND and electron density by high-resolution XRD, supported by *ab initio* calculations, provides complementary insights into the electronic and magnetic structure of the mixed-valent diruthenium(II,III) tetracarboxylate complex. The charge-density maps show the distribution of electron density, which is mainly localised on the ruthenium centres, with no significant density in between. However, they also indicate partial delocalisation from the ruthenium centres towards the bromido and carboxylato ligands. Experimental topological analysis of the Ru···Ru bond shows an open-shell metal–metal interaction, in agreement with the $\sigma^2\pi^4\delta^2(\pi^*\delta^*)^3$ electronic configuration. Quantum calculations indicate similar delocalized spin populations on both oxygen and bromido ligands. In contrast, the spin-density maps show that the unpaired electrons are predominantly localized on the ruthenium atoms. This suggest that the delocalized spin density on oxygen and bromido ligands lies beyond the detection limit of our PND experiment.

The local magnetic susceptibility tensors derived from PND show planar anisotropy aligned with the equatorial oxygen atoms and a hard axis along the Ru–Ru bonds, highlighting the strong influence of the oxygen geometry on the anisotropy. These observations are fully consistent with bulk magnetic data, which show an easy magnetization axis along the crystallographic *c* axis and a hard axis along the *b* axis, but provide a more detailed, atomically resolved description of the magnetic anisotropy.

Moreover, the experimental electron density obtained from high-resolution XRD and the experimental magnetic anisotropy derived from PND show that the valence shell of diruthenium B is more contracted, and this leads to the hypothesis that diruthenium B is a slightly more localized mixed-valence system than diruthenium A but still a delocalised mixed-valence system of class III with a spin state of $S = 3/2$. This result demonstrates the value and power of such a study, combining advanced crystallographic methods for the determination of experimental electron and spin densities and magnetic anisotropy, as these details could not be obtained from a classical crystallographic structure even when combined with magnetometry measurements.

Author contributions

Haruki Yairi and Torao Fujimoto: investigation. Sabrina Grenda, Oscar Fabelo, Iurii Kibalin, Nicolas Claiser, Rémi Maurice, Arsen Gukasov, Laura Canadillas-Delgado, José A. Rodriguez Velamazan, Jean-François Jacquot, Ryoji Mitsuhashi, Masahiro Mikuriya, Makoto Handa: investigation, writing, reviewing & editing. Dominique Luneau: supervision, investigation, writing, reviewing & editing.

Conflicts of interest

There are no conflicts to declare.

Data availability

Supplementary information (SI): experimental details on the synthesis, characterization and crystal growing of (NBu_4) $[Ru_2^{V}(O_2C_3CH_7)_4Br_2]$, high-resolution X-ray diffraction crystal structure, experimental electron density model, magnetic measurements, neutron diffraction, polarized neutron diffraction, experimental spin density model and magnetic susceptibility tensor determination, and quantum mechanical calculations complemented by additional tables and figures for the crystal structures' electron density, spin density and magnetism; X-ray crystallographic data with embedded multipole model and experimental structure factors and non-polarised neutron data. See DOI: https://doi.org/10.1039/d6dt00342g.

The authors have cited additional references within SI.[23,42,66,71–73,75–90]

CCDC 2516707 and 2519322 contain the supplementary crystallographic data for this paper.[91a,b]

Acknowledgements

Dedication: The authors dedicate this paper to Beatrice Gillon for her seminal work in polarised neutron diffraction of magnetic coordination compounds.

Low-temperature high-resolution X-Ray diffraction on single-crystal was carried out at the PMD2X X-ray diffraction facility of the CRM2 laboratory (Université de Lorraine) for (https://www.crm2.univ-lorraine.fr/plateformes/pmd2x/). Polarised and non-polarized neutron diffraction experiments were performed on the D3 and D19 diffractometers respectively, run by the Institut Laue-Langevin (ILL). Beamtimes at Institut Laue-Langevin (ILL) were granted under the proposals number 5-51-584 (https://doi.org/10.5291/ILL-DATA.5-51-584) and 5-51-564 (https://doi.org/10.5291/ILL-DATA.5-51-564). We thank Dr Frédéric Guégan for discussion and participation in preliminary data collection. This work was partially supported by JSPS KAKENHI Grant Number JP24K08363 and Region Auvergne-Rhône-Alpes and its programme "Ambition Internationale 2025" Grant number 00283799-1.

References

1 T. A. Stephenson and G. Wilkinson, New Ruthenium Carboxylate Complexes, *J. Inorg. Nucl. Chem.*, 1966, **28**, 2285–2291.
2 M. J. Bennett, K. G. Caulton and F. A. Cotton, Structure of Tetra-N-Butyratodiruthenium Chloride a Compound with a Strong Metal-Metal Bond, *Inorg. Chem.*, 1969, **8**, 1–6.
3 F. A. Cotton, N. F. Curtis, B. F. G. Johnson, J. T. Mague, J. S. Wood, C. B. Harris, W. R. Robinson and S. J. Lippard, Mononuclear + Polynuclear Chemistry of Rhenium (3) - Its Pronounced Homophilicity, *Science*, 1964, **145**, 1305–1307.
4 F. A. Cotton and D. G. Nocera, The whole story of the two-electron bond, with the delta bond as a paradigm, *Acc. Chem. Res.*, 2000, **33**, 483–490.
5 R. J. H. Clark and M. L. Franks, Resonance Raman-Spectra of Chlorotetra-Acetato-Diruthenium and Chlorotetrabutyrato-Diruthenium, *Dalton Trans.*, 1976, 1825–1828.
6 F. A. Cotton and E. Pedersen, Magnetic and Electrochemical Properties of Transition Metal Complexes with Multiple Metal-to-Metal Bonds. II. $[Ru_2(C_3H_7COO)_4]^{n+}$ with n = 0 and 1, *Inorg. Chem.*, 1975, **14**, 388–391.
7 J. G. Norman, G. E. Renzoni and D. A. Case, Electronic-structure of $Ru_2(O_2CR)_4^+$ and $Rh_2(O_2CR)_4^+$ complexes, *J. Am. Chem. Soc.*, 1979, **101**, 5256–5267.
8 C. R. Wilson and H. Taube, Acetate Complexes of Dirhodium and Diruthenium - Aquation and Reduction-Oxidation, *Inorg. Chem.*, 1975, **14**, 2276–2279.
9 J. Telser and R. S. Drago, Reinvestigation of the Electronic and Magnetic-Properties of Ruthenium Butyrate Chloride, *Inorg. Chem.*, 1984, **23**, 3114–3120.
10 M. A. S. Aquino, Diruthenium and diosmium tetracarboxylates: synthesis, physical properties and applications, *Coord. Chem. Rev.*, 1998, **170**, 141–202.
11 P. Angaridis, in *Multiple Bonds Between Metal Atoms*, ed. F. A. Cotton, C. A. Murillo and R. A. Walton, Springer US, Boston, MA, 2005, pp. 377–430.
12 M. Mikuriya, D. Yoshioka and M. Handa, Magnetic interactions in one-, two-, and three-dimensional assemblies of dinuclear ruthenium carboxylates, *Coord. Chem. Rev.*, 2006, **250**, 2194–2211.
13 M. B. Robin and P. Day, Mixed Valence Chemistry-A Survey and Classification, *Adv. Inorg. Chem. Radiochem.*, 1968, **10**, 247–422.
14 L. R. Falvello, B. M. Foxman and C. A. Murillo, Fitting the Pieces of the Puzzle: The delta Bond, *Inorg. Chem.*, 2014, **53**, 9441–9456.
15 M. Handa, Y. Sayama, M. Mikuriya, R. Nukada, I. Hiromitsu and K. Kasuga, Structure and magnetic properties of a chain complex with alternating Ru(II,III) dimer and nitroxide radical arrangement Ru-2(O2CCMe3)(4)(nitph) (n)(BF4)(n), nitph = 2-phenyl-4,4,5,5-tetramethyl-4,5-dihydro-1H-imidazol-1-oxyl 3-N-oxide, *Bull. Chem. Soc. Jpn.*, 1998, **71**, 119–125.

16 F. D. Cukiernik, D. Luneau, J. C. Marchon and P. Maldivi, Mixed-valent diruthenium long-chain carboxylates. 2. Magnetic properties, *Inorg. Chem.*, 1998, **37**, 3698–3704.
17 R. Jimenez-Aparicio, F. A. Urbanos and J. M. Arrieta, Magnetic properties of diruthenium(II,III) carboxylate compounds with large zero-field splitting and strong antiferromagnetic coupling, *Inorg. Chem.*, 2001, **40**, 613–619.
18 W. W. Shum, Y. Liao and J. S. Miller, Zero-field splitting, field-dependent magnetization of mixed-varent S = 3/2 diruthenium(II,III) tetracarboxylates, *J. Phys. Chem. A*, 2004, **108**, 7460–7462.
19 M. Mikuriya, K. Tanaka, M. Handa, I. Hiromitsu, D. Yoshioka and D. Luneau, Adduct complexes of ruthenium(II,III) propionate dimer with pyridyl nitroxides, *Polyhedron*, 2005, **24**, 2658–2664.
20 M. Mikuriya, D. Yoshioka, A. Borta, D. Luneau, D. Matoga, J. Szklarzewicz and M. Handa, Molecule-based magnetic materials based on dinuclear ruthenium carboxylate and octacyanotungstate, *New J. Chem.*, 2011, **35**, 1226–1233.
21 M. Mikuriya, D. Yoshioka, D. Luneau, S. Kawauchi, D. Matoga, J. Szklarzewicz and M. Handa, Tetra(n-butyl) ammonium salt of a ferrimagnetic complex based on mixed-valent dinuclear ruthenium pivalate and octacyanidotungstate(V), *C. R. Chim.*, 2019, **22**, 476–482.
22 Y. Hiraoka, T. Ikeue, H. Sakiyama, F. Guegan, D. Luneau, B. Gillon, I. Hiromitsu, D. Yoshioka, M. Mikuriya, Y. Kataoka and M. Handa, An unprecedented up-field shift in the ^{13}C NMR spectrum of the carboxyl carbons of the lanterntype dinuclear complex TBA[$Ru_2(O_2CCH_3)_4Cl_2$] (TBA+ = tetra(n-butyl)ammonium cation), *Dalton Trans.*, 2015, **44**, 13439–13443.
23 N. K. Hansen and P. Coppens, Testing aspherical atom refinements on small-molecule data sets, *Acta Crystallogr., Sect. A*, 1978, **34**, 909–921.
24 P. Macchi, Modern charge density studies: the entanglement of experiment and theory, *Crystallogr. Rev.*, 2013, **19**, 58–101.
25 P. Macchi, J. M. Gillet, F. Taulelle, J. Campo, N. Claiser and C. Lecomte, Modelling the experimental electron density: only the synergy of various approaches can tackle the new challenges, *IUCrJ*, 2015, **2**, 441–451.
26 L. J. Farrugia, P. R. Mallinson and B. Stewart, Experimental charge density in the transition metal complex $Mn_2(CO)_{10}$: a comparative study, *Acta Crystallogr., Sect. B: Struct. Sci.*, 2003, **59**, 234–247.
27 U. Flierler and D. Stalke, in *Electron Density and Chemical Bonding I: Experimental Charge Density Studies*, ed. D. Stalke, Springer Berlin Heidelberg, Berlin, Heidelberg, 2012, pp. 1–20.
28 R. F. W. Bader, *Atoms in Molecules: A Quantum Theory*, Oxford University Press, 1990.
29 C. Lecomte, M. Souhassou and S. Pillet, Topology of experimental charge density: a tool for understanding atomic interactions, *J. Mol. Struct.*, 2003, **647**, 53–64.
30 A. B. Voufack, A. B. Dippenaar, C. Esterhuysen, D. A. Haynes, M. Souhassou, C. Lecomte and N. Claiser, Experimental Charge Density Analysis of p-$O_2NC_6F_4CNSSN^{\bullet}$, a Dithiadiazolyl Molecular Radical, *Cryst. Growth Des.*, 2024, **24**, 8736–8747.
31 B. Gillon, The classical flipping ratio technique applied to non classical magnetic materials: Molecule-based and Photoswitchable magnetic compounds, *J. Phys.*, 2007, 1–30.
32 J. Schweizer, Spin densities in magnetic molecular compounds, *Phys. B*, 1997, **234**, 772–779.
33 A. Zheludev, A. Grand, E. Ressouche, J. Schweizer, B. G. Morin, J. A. Epstein, D. A. Dixon and J. S. Miller, The Spin-Density Distribution in the Tetracyanoethylene Radical-Anion, TCNE (Center-Dot-), by Single-Crystal Polarized Neutron-Diffraction, *Angew. Chem., Int. Ed. Engl.*, 1994, **33**, 1397–1399.
34 B. Gillon, C. Mathoniere, E. Ruiz, S. Alvarez, A. Cousson, T. M. Rajendiran and O. Kahn, Spin densities in a ferromagnetic bimetallic chain compound: Polarized neutron diffraction and DFT calculations, *J. Am. Chem. Soc.*, 2002, **124**, 14433–14441.
35 . C. Aronica, Y. Chumakov, E. Jeanneau, D. Luneau, P. Neugebauer, A. L. Barra, B. Gillon, A. Goujon, A. Cousson, J. Tercero and E. Ruiz, Structure, Magnetic Properties, Polarized Neutron Diffraction, and Theoretical Study of a Copper(II) Cubane, *Chem. – Eur. J.*, 2008, **14**, 9540–9548.
36 J. A. Rodriguez-Velamazan, J. S. Costa, J. K. Tang, P. Gamez, J. Campo and J. Luzon, Internal magnetic structure of a Mn3 cluster determined by polarised neutron diffraction, *Acta Crystallogr., Sect. A: Found. Crystallogr.*, 2008, **64**, C571.
37 Y. Kousaka, T. Koyama, K. Ohishi, K. Kakurai, V. Hutanu, H. Ohsumi, T. Arima, A. Tokuda, M. Suzuki, N. Kawamura, A. Nakao, T. Hanashima, J. Suzuki, J. Campo, Y. Miyamoto, A. Sera, K. Inoue and J. Akimitsu, Monochiral helimagnetism in homochiral crystals of $CsCuCl_3$, *Phys. Rev. Mater.*, 2017, **1**, 071402.
38 O. Kahn, Magnetic anisotropy in molecule-based magnets, *Philos. Trans. R. Soc., A*, 1999, **357**, 3005–3023.
39 A. Cornia, D. Gatteschi and R. Sessoli, New experimental techniques for magnetic anisotropy in molecular materials, *Coord. Chem. Rev.*, 2001, **219**, 573–604.
40 A. Gukasov and P. J. Brown, Determination of atomic site susceptibility tensors from polarized neutron diffraction data, *J. Phys.: Condens. Matter*, 2002, **14**, 8831–8839.
41 F. Guegan, J. Jung, B. Le Guennic, F. Riobe, O. Maury, B. Gillon, J. F. Jacquot, Y. Guyot, C. Morell and D. Luneau, Evidencing under-barrier phenomena in a Yb(III) SMM: a joint luminescence/neutron diffraction/SQUID study, *Inorg. Chem. Front.*, 2019, **6**, 3152–3157.
42 O. Iasco, Y. Chumakov, F. Guegan, B. Gillon, M. Lenertz, A. Bataille, J. F. Jacquot and D. Luneau, Mapping the Magnetic Anisotropy inside a Ni-4 Cubane Spin Cluster Using Polarized Neutron Diffraction, *Magnetochemistry*, 2017, **3**, 25.
43 K. Ridier, B. Gillon, A. Gukasov, G. Chaboussant, A. Cousson, D. Luneau, A. Borta, J. F. Jacquot, R. Checa, Y. Chiba, H. Sakiyama and M. Mikuriya, Polarized Neutron

Diffraction as a Tool for Mapping Molecular Magnetic Anisotropy: Local Susceptibility Tensors in Co-II Complexes, *Chem. – Eur. J.*, 2016, **22**, 724–735.

44 D. Luneau and B. Gillon, Polarized Neutron Diffraction: An Excellent Tool to Evidence the Magnetic Anisotropy-Structural Relationships in Molecules, *Magnetochemistry*, 2021, **7**, 158.

45 E. A. Klahn, C. Gao, B. Gillon, A. Gukasov, X. Fabreges, R. O. Piltz, S. D. Jiang and J. Overgaard, Mapping the Magnetic Anisotropy at the Atomic Scale in Dysprosium Single-Molecule Magnets, *Chem. – Eur. J.*, 2018, **24**, 16576–16581.

46 K. Ridier, A. Mondal, C. Boilleau, O. Cador, B. Gillon, G. Chaboussant, B. Le Guennic, K. Costuas and R. Lescouezec, Polarized Neutron Diffraction to Probe Local Magnetic Anisotropy of a Low-Spin Fe(III) Complex, *Angew. Chem., Int. Ed.*, 2016, **55**, 3963–3967.

47 T. Kimura, T. Sakurai, M. Shima, T. Togano, M. Mukaida and T. Nomura, Structure of Tetra-μ-Formatodiruthenium Bromide, *Bull. Chem. Soc. Jpn.*, 1982, **55**, 3927–3928.

48 M. C. Barral, R. Gonzalez-Prieto, S. Herrero, R. Jimenez-Aparicio, J. L. Priego, M. R. Torres and F. A. Urbanos, Anionic dihalotetraacetatodiruthenium(II,III) compounds, *Polyhedron*, 2005, **24**, 239–247.

49 M. C. Barral, R. Gonzalez-Prieto, R. Jimenez-Aparicio, J. L. Priego, E. C. Royer, M. R. Torres and F. A. Urbanos, Tetra(3-methoxypropionato)diruthenium(II,III) Units: Supramolecular Organization in the Complex $[Ru_2(\mu\text{-}O_2CCH_2CH_2OMe)_4(H_2O)_2]BF_4$, *Z. Anorg. Allg. Chem.*, 2005, **631**, 2075–2080.

50 M. C. Barral, R. Gonzalez-Prieto, R. Jimenez-Aparicio, J. L. Priego, M. R. Torres and F. A. Urbanos, Synthesis, properties, and structural characterization of bromo- and iodotetracarboxylatodiruthenium(II,III) compounds, *Eur. J. Inorg. Chem.*, 2004, 4491–4501.

51 D. Olea, R. Gonzalez-Prieto, J. L. Priego, M. C. Barral, P. J. de Pablo, M. R. Torres, J. Gomez-Herrero, R. Jimenez-Aparicio and F. Zamora, MMX polymer chains on surfaces, *Chem. Commun.*, 2007, 1591–1593.

52 L. C. Wu, C. W. Hsu, Y. C. Chuang, G. H. Lee, Y. C. Tsai and Y. Wang, Bond Characterization on a Cr-Cr Quintuple Bond: A Combined Experimental and Theoretical Study, *J. Phys. Chem. A*, 2011, **115**, 12602–12615.

53 K. Tahara, T. Morino, Y. Morimoto, Y. Nakamura, K. Sugimoto, Y. Ozawa and M. Abe, Synthetic, Electrochemical, DFT, and Synchrotron X-ray Charge-Density Studies on Oxo-centered Triruthenium Clusters Supported by Electron-Withdrawing Carboxylates, *Inorg. Chem.*, 2024, **63**, 19087–19097.

54 L. C. Wu, T. C. Weng, I. J. Hsu, Y. H. Liu, G. H. Lee, L. Jyh-Fu and Y. Wang, Chemical Bond Characterization of a Mixed-Valence Tri-Cobalt Complex, $Co_3(\mu\text{-admtrz})4(\mu\text{-}OH)_2(CN)_6{\cdot}2H_2O$, *Inorg. Chem.*, 2013, **52**, 11023–11033.

55 R. D. Poulsen, J. Overgaard, A. Schulman, C. Ostergaard, C. A. Murillo, M. A. Spackman and B. B. Iversen, Effects of Weak Intermolecular Interactions on the Molecular Isomerism of Tricobalt Metal Chains, *J. Am. Chem. Soc.*, 2009, **131**, 7580–7591.

56 C. R. Lee, C. C. Wang, K. C. Chen, G. H. Lee and Y. Wang, Bond characterization of metal squarate complexes MII $(C_4O_4)(H_2O)_4$; M = Fe, Co, Ni, Zn, *J. Phys. Chem. A*, 1999, **103**, 156–165.

57 I. Stepanenko, P. Mizetskyi, E. Orlowska, L. Bucinsky, M. Zalibera, B. Vénosová, M. Clémancey, G. Blondin, P. Rapta, G. Novitchi, W. Schrader, D. Schaniel, Y. S. Chen, M. Lutz, J. Kozísek, J. Telser and V. B. Arion, The Ruthenium Nitrosyl Moiety in Clusters: Trinuclear Linear μ-Hydroxido Magnesium(II)-Diruthenium(II), μ3-Oxido Trinuclear Diiron(III)-Ruthenium(II), and Tetranuclear μ4-Oxido Trigallium(III)-Ruthenium(II) Complexes, *Inorg. Chem.*, 2022, **61**, 950–967.

58 C. Lepetit, P. Fau, K. Fajerwerg, M. L. Kahn and B. Silvi, Topological analysis of the metal-metal bond: A tutorial review, *Coord. Chem. Rev.*, 2017, **345**, 150–181.

59 J. F. Van der Maelen and J. A. Cabeza, A topological analysis of the bonding in $M_2(CO)_{10}$ and $M_3(\mu\text{-}H)_3(CO)_{12}$ complexes (M = Mn, Tc, Re), *Theor. Chem. Acc.*, 2016, **135**, 64.

60 C. Gatti and D. Lasi, Source function description of metal-metal bonding in d-block organometallic compounds, *Faraday Discuss.*, 2007, **135**, 55–78.

61 L. J. Farrugia and P. Macchi, in *Electron Density and Chemical Bonding I: Experimental Charge Density Studies*, ed. D. Stalke, 2012, vol. 146, pp. 127–158.

62 A. P. Ginsberg and M. E. Lines, Magnetic Exchange in Transition Metal Complexes. VIII. Molecular Field Theory of Intercluster Interactions in Transition Metal Cluster Complexes, *Inorg. Chem.*, 1972, **11**, 2289–2290.

63 R. J. Papoular and B. Gillon, Maximum-Entropy Reconstruction of Spin-Density Maps in Crystals from Polarized Neutron-Diffraction Data, *Europhys. Lett.*, 1990, **13**, 429–434.

64 P. Schleger, A. PuigMolina, E. Ressouche, O. Rutty and J. Schweizer, A general maximum-entropy method for model-free reconstructions of magnetization densities from polarized neutron diffraction data, *Acta Crystallogr., Sect. A: Found. Crystallogr.*, 1997, **53**, 426–435.

65 K. D. Demadis, C. M. Hartshorn and T. J. Meyer, The Localized-to-Delocalized Transition in Mixed-Valence Chemistry, *Chem. Rev.*, 2001, **101**, 2655–2686.

66 B. O. Roos, A. C. Borin and L. Gagliardi, Reaching the maximum multiplicity of the covalent chemical bond, *Angew. Chem., Int. Ed.*, 2007, **46**, 1469–1472.

67 N. Fritsch, C. R. Wick, T. Waidmann, P. O. Dral, J. Tucher, F. W. Heinemann, T. E. Shubina, T. Clark and N. Burzlaff, Multiply Bonded Metal(II) Acetate (Rhodium, Ruthenium, and Molybdenum) Complexes with the trans-1,2-Bis(N-methylimidazol-2-yl)ethylene Ligand, *Inorg. Chem.*, 2014, **53**, 12305–12314.

68 A. D. Becke, Density-functional thermochemistry. III. The role of exact exchange, *J. Chem. Phys.*, 1993, **98**, 5648–5652.

69 C. T. Lee, W. T. Yang and R. G. Parr, Development of the Colle-Salvetti Correlation-Energy Formula into a Functional

of the Electron-Density, *Phys. Rev. B: Condens. Matter Mater. Phys.*, 1988, **37**, 785–789.

70 P. J. Stephens, F. J. Devlin, C. F. Chabalowski and M. J. Frisch, *Ab initio* Calculation of Vibrational Absorption and Circular-Dichroism Spectra Using Density-Functional Force-Fields, *J. Phys. Chem.*, 1994, **98**, 11623–11627.

71 R. Maurice, R. Bastardis, C. de Graaf, N. Suaud, T. Mallah and N. Guihéry, Universal Theoretical Approach to Extract Anisotropic Spin Hamiltonians, *J. Chem. Theory Comput.*, 2009, **5**, 2977–2984.

72 C. Angeli, R. Cimiraglia, S. Evangelisti, T. Leininger and J. P. Malrieu, Introduction of n-electron valence states for multireference perturbation theory, *J. Chem. Phys.*, 2001, **114**, 10252–10264.

73 C. Angeli, R. Cimiraglia and J. P. Malrieu, N-electron valence state perturbation theory:: a fast implementation of the strongly contracted variant, *Chem. Phys. Lett.*, 2001, **350**, 297–305.

74 C. G. Pech, P. A. B. Haase, N. Galland, A. Borschevsky and R. Maurice, Relevance of effective bond orders in hetero-diatomic molecules and role of the spin-orbit coupling in the AtX (X = At – F) series, *Phys. Rev. A*, 2019, **100**, 032518.

75 Agilent, *CrysAlis PRO*, Agilent Technologies Ltd, Yarnton, Oxfordshire, England, 2014.

76 F. H. Allen, Systematic Pairwise Comparison of Geometric Parameters Obtained by X-Ray and Neutron-Diffraction, *Acta Crystallogr., Sect. B: Struct. Sci.*, 1986, **42**, 515–522.

77 F. H. Allen and I. J. Bruno, Bond lengths in organic and metal-organic compounds revisited: X-H bond lengths from neutron diffraction data, *Acta Crystallogr., Sect. B: Struct. Sci.*, 2010, **66**, 380–386.

78 R. H. Blessing, Data Reduction and Error Analysis for Accurate Single Crystal Diffraction Intensities, *Crystallogr. Rev.*, 1987, **1**, 3–58.

79 L. J. Bourhis, O. V. Dolomanov, R. J. Gildea, J. A. K. Howard and H. Puschmann, The Anatomy of a Comprehensive Constrained, Restrained, Refinement Program for the Modern Computing Environment - Olex2 Disected, *Acta Crystallogr., Sect. A: Found. Adv.*, 2015, **71**, 59–71.

80 E. Clementi and D. L. Raimondi, Atomic Screening Constants from SCF Functions, *J. Chem. Phys.*, 1963, **38**, 2686–2689.

81 O. V. Dolomanov, L. J. Bourhis, R. J. Gildea, J. A. K. Howard and H. Puschmann, OLEX2: a complete structure solution, refinement and analysis program, *J. Appl. Crystallogr.*, 2009, **42**, 339–341.

82 M. Douglas and N. M. Kroll, Quantum Electrodynamical Corrections to Fine-Structure of Helium, *Ann. Phys.*, 1974, **82**, 89–155.

83 B. Guillot, L. Viry, R. Guillot, C. Lecomte and C. Jelsch, Refinement of proteins at subatomic resolution with MOPRO, *J. Appl. Crystallogr.*, 2001, **34**, 214–223.

84 M. Handa, H. Yairi, Y. Koyama, R. Mitsuhashi and M. Mikuriya, Polynuclear Chain Compound of Tetrakis(mu-n-butyrato-O,O′)diruthenium Bromide, *X-Ray Struct. Anal. Online*, 2022, **38**, 21–23.

85 G. Jansen and B. A. Hess, Revision of the Douglas-Kroll Transformation, *Phys. Rev. A*, 1989, **39**, 6016–6017.

86 F. Neese, Efficient and accurate approximations to the molecular spin-orbit coupling operator and their use in molecular g-tensor calculations, *J. Chem. Phys.*, 2005, **122**, 034107.

87 D. A. Pantazis, X. Y. Chen, C. R. Landis and F. Neese, All-electron scalar relativistic basis sets for third-row transition metal atoms, *J. Chem. Theory Comput.*, 2008, **4**, 908–919.

88 B. O. Roos, P. R. Taylor and P. E. M. Siegbahn, Complete Active Space SCF Method (CASSCF) Using a Density-Matrix Formulated Super-CI Approach, *Chem. Phys.*, 1980, **48**, 157–173.

89 G. M. Sheldrick, SHELXT - Integrated space-group and crystal-structure determination, *Acta Crystallogr., Sect. A: Found. Adv.*, 2015, **71**, 3–8.

90 G. M. Sheldrick, Crystal structure refinement with SHELXL, *Acta Crystallogr., Sect. C: Struct. Chem.*, 2015, **71**, 3–8.

91 (*a*) CCDC 2516707: Experimental Crystal Structure Determination, 2026, DOI: 10.5517/ccdc.csd.cc2qgv35; (*b*) CCDC 2519322: Experimental Crystal Structure Determination, 2026, DOI: 10.5517/ccdc.csd.cc2qkkgb.